ORIGINAL ARTICLE

Molecular design of azo-carbazole monolithic dyes for updatable full-color holograms

Kenji Kinashi[1], Takahiro Fukami[2], Yuki Yabuhara[2], Satsuki Motoishi[3], Wataru Sakai[1], Masuki Kawamoto[4], Takafumi Sassa[4] and Naoto Tsutsumi[1]

For the use of updatable full-color holography in practical applications, azo-carbazole (ACzE) monolithic dyes dispersed in poly (methyl methacrylate) (PMMA) films with high diffraction efficiency, write/delete capabilities and transparency are of extreme importance. We synthesized seven types of novel ACzE monolithic dyes and examined the influence of substituents introduced in the *para* position of the phenyl ring and the distinct strength of the substituents (NO_2: NACzE, CN: CACzE, CH_3CO: AACzE, F: FACzE, CH_3O: MACzE, OH: HACzE and NH_2: AmACzE) on the phenyl ring of the ACzEs. Spectroscopic and holographic optical properties, including absorption coefficient α, wavelength dependence of diffraction efficiency η, response time τ, the thickness of the recorded gratings d, the Bragg angle $\Delta\vartheta$ and the Q-factor, required for the optimization of updatable full-color holograms were investigated. On the basis of the spectroscopic and holographic optical results, the appropriate writing/reading beams were determined as follows: $561/>600$ nm for NACzE, $532/>560$ nm for CACzE (and AACzE), $491/>530$ nm for MACzE (and HACzE). According to the spectroscopic and holographic optical results, we propose here an insight designed to allow updatable full-color holography using ACzEs, and demonstrate a multi-color hologram in MACzE/PMMA.
NPG Asia Materials (2016) **8**, e311; doi:10.1038/am.2016.136; published online 16 September 2016

INTRODUCTION

An updatable full-color hologram is the ultimate imaging technology. The term holography is taken from the Greek words, holos (whole) and graphe (writing or drawing). Unlike pseudo-three-dimensional (3D) images or virtual reality on a two-dimensional computer display, a hologram is a truly 3D and freestanding image that does not simulate spatial depth nor require a special viewing device. Theoretically, holograms could someday be transmitted electronically to a special display device in your home and business. Unfortunately, current holographic technology has not lived up to expectations, which were largely driven by the science fiction portrayed in the 'Star Wars' film in 1977. Today, the main applications of holograms are in the fields of security and authentication for branding, bank notes, and passports, among other applications. Holographic imaging is largely consigned to artistic exhibitions or specialized optical components. Practical applications of dynamic (updatable) full-color holograms have many issues that remain to be resolved; one of which is the extreme difficulty of designing materials that can accommodate updatable full-color holography.

Organic molecules have attracted particular attention for use in updatable holography. In addition, other photonic applications such as holographic memory, optical switches and waveguides have been proposed.[1–5] Examples of updatable holography include azobenzene molecules in polymer matrices,[6–8] liquid crystals,[9,10] polymeric liquid crystals[11–15] and photorefractive polymers.[16–19] In particular, azobenzene molecules are the most promising candidates for use in updatable holography because azobenzenes are well-known photosensitive chromophores that undergo *trans–cis* photoisomerization upon irradiation with light of an appropriate wavelength in a solution or in an appropriate host matrix.[20–24] The repetition of such photoisomerization within a host matrix leads to perpendicular alignment of the long axis of the azobenzene chromophore to the electric field vector of the linearly polarized light, which eventually induces anisotropy. Therefore, azobenzene-functionalized polymers have attracted considerable attention due to their large refractive index anisotropy induced by linearly polarized light irradiation below the glass transition temperature.[25,26]

We previously developed updatable red-colored holograms using an NO_2-substituted azo-carbazole (**ACzE**) monolithic dye, 3-[(4-nitro-phenyl)azo]-9*H*-carbazole-9-ethanol (**NACzE**), dispersed in poly (methyl methacrylate) (PMMA),[27–29] and proposed a relationship between the holographic properties and isosbestic point. However, the spectroscopic and optical characteristics of the **ACzE** monolithic dyes are not yet thoroughly understood.

In this study, our motivation was to discover novel azobenzene dyes that contained **ACzE** as their basic molecular structure for use in updatable holography with the following intended colors: red, yellow, green, blue and even full color. For this purpose, we investigated the

influence of introducing substituents in the *para* position of the phenyl ring as well as the distinct strength of the substituents (NO_2, CN, CH_3CO, F, CH_3O, OH and NH_2) on the phenyl ring. Furthermore, we proposed a design that allows updatable full-color holography utilizing **ACzE** monolithic dyes on the basis of the spectroscopic and optical results.

MATERIALS AND METHODS

The 3-(phenylazo)-9*H*-carbazole-9-ethanols (**ACzEs**) with different substituents on the phenyl group (**NACzE**, **CACzE**, **AACzE**, **FACzE**, **MACzE**, **HACzE** and **AmACzE**) were synthesized as shown in Scheme 1. The **ACzEs** with an NO_2, CN and CH_3CO substituent (**NACzE**, **CACzE** and **AACzE**) were synthesized by an azo-coupling reaction. The **ACzE** with an NH_2 substituent (**AmACzE**) was synthesized in an ammonium chloride solution containing Fe powder.[30] The **HACzE** was methoxylated to produce the **ACzE** with a CH_3O substituent (**MACzE**). The **ACzE** with an F substituent (**FACzE**) was synthesized from the **AmACzE** according to ta Balz–Schiemann reaction.[31] The **ACzE** with an OH substituent (**HACzE**) was produced through an Ullmann reaction,[32] a Pd-catalyzed reaction that forms a carbazole structure, and a reduction reaction to add the amine substituent to the carbazole, followed by an azo-coupling reaction with a phenol. The **HACzE** was methoxylated to produce the **ACzE** with a CH_3O substituent (**MACzE**). The chemical structures of the products were characterized by ^{1}H-nuclear magnetic resonance (^{1}H-NMR) (and ^{13}C-NMR; AV-600, Bruker BioSpin Inc., Billerica, MA, USA, 600 MHz, tetramethylsilane—TMS—as an internal standard), Fourier transform infrared (FT/IR-4700, Jasco Co., Tokyo, Japan) and time-of-flight mass spectrometry (MicroTOF, Bruker Daltonics Inc., Billerica, MA, USA). Melting points (mp) were determined using a melting-point apparatus (MP-500P, Yanaco, Kyoto, Japan) with a digital thermometer. Detailed synthesis procedures and the melting point for each **ACzE**, and assignment of each compound by NMR, mass and Fourier transform infrared spectroscopy are summarized in the Supplementary Information. Especially, ^{13}C-NMR spectra of **ACzEs** are shown in Supplementary Figure S1

PMMA with a molecular weight of ca. 100 000 g mol^{-1} was used for the polymer matrix. Several approaches were used to incorporate azobenzene chromophores into polymer matrices: random incorporation (guest–host systems), binding to main or side chains or formation of thin-layer structures such as Langmuir–Blodgett films. In this study, we employed the guest–host system for the **ACzE**/PMMA films and used one of the better known ratios for an azo-carbazole/PMMA system (30/70 wt%).[33,34] The **ACzE** monolithic dyes with different substituents, NO_2, CN, CH_3CO, F, CH_3O, OH and NH_2, were mixed with PMMA in tetrahydrofuran. The mixtures were left stirring overnight and then cast on a hot plate at 70 °C for 24 h. The obtained composites were sandwiched between two glass plates at 240 °C. The thickness of the composite films was controlled to ca. 80 μm by inserting polyimide spacers. Ultraviolet−visible absorption spectra were obtained using a Lambda 1050 UV/Vis/NIR spectrophotometer (PerkinElmer, Waltham, MA, USA). The absorption coefficient α is given by $\alpha = A\ln(10)/d$, where A is the measured absorbance and d is the thickness of the sample. The isosbestic point was measured after the sample films were irradiated by a mercury lamp.

The diffraction efficiency was measured using a non-degenerate four-wave mixing technique with six different writing lasers at 632.8, 594, 561, 532, 491 and 473 nm. Another laser at 632.8 nm was used as a reading (probe) beam. The two writing laser beams of *p*-polarization were intersected on the sample surface at angles of − 7.5° and 7.5°. The weak intensity of the *p*-polarized reading beam probed the refractive index gratings in the sample from the direction opposite to one side of the writing beams. We used the intensities of a transmitted beam (I_t) and diffracted beam (I_d) to calculate the internal diffraction efficiency η with equation (1):

$$\eta\% = \frac{I_d}{I_t + I_d} \times 100 \tag{1}$$

The angular selectivity of the recorded gratings for different writing beam wavelengths was recorded using the geometry shown in Supplementary Figure S2. Laser sources for writing were 25 mW diode-pumped solid-state lasers: Blues at 473 nm, Calypso at 491 nm, Samba at 532 nm, Jive at 561 nm

and Mambo at 594 nm (Cobolt, Solna, Sweden), and a 10 mW He–Ne laser at 632.8 nm (CVI Melles Griot, Albuquerque, NM, USA). The probe laser for reading was a 10 mW He–Ne laser (LASOS Lasertechnik GmbH, Jena, Germany). The sample was fixed on a rotation stage at 0°, so that the normal angle crossed the axial bisector of the two writing beams. The recording process was the same as for the non-degenerate four-wave mixing setup. The intensity of the reading beam at 632.8 nm was monitored rotationally on a maximum center angle θ_{max} that corresponded to the Bragg-matched diffraction efficiency ($\xi = 0$). Calculations based on the semi-empirical molecular orbital theory AM1 for 3D-optimized structures and their highest occupied molecular orbital (HOMO) π-electron clouds were performed using WinMOPAC 3.0 software (Fujitsu, Tokyo, Japan).

A multi-color hologram was reproduced using an updatable multi-color holographic display system. The original image was divided into red and green color images using a HOLOEYE DVI video signal splitter, and each image on a spatial light modulator (Pluto, 1920 × 1080 pixel resolution and 8.0 μm pixel size, HOLOEYE Photonics AG, Berlin-Adlershof, Germany) was recorded in a **MACzE**/PMMA film device using a single longitudinal mode blue laser (Genesis CX-488-2000, 488 nm, 2 W, Coherent Inc., Santa Clara, CA, USA). The color hologram was reproduced using a green laser (OBIS 532 nm, 100 mW, Coherent Inc.) and a red laser (diode-pumped solid-state laser series 640 nm, 100 mW, LASOS Lasertechnik GmbH).

RESULTS AND DISCUSSION
Optical properties
The structure of the **ACzEs** and the ultraviolet–visible absorption spectra of the **ACzEs** in PMMA are shown in Figure 1. The spectra of the **ACzE**/PMMA films contain a broad absorption region that extends from 350 to 600 nm. **NACzE** has a maximum at 440 nm, **CACzE** has a maximum at 426 nm, **AACzE** has a maximum at 415 nm, **MACzE** has a maximum at 394 nm, **HACzE** has a maximum at 395 nm, **FACzE** has a maximum at 395 nm and **AmACzE** has a maximum at 410 nm, which are attributed to $\pi - \pi^*$ transitions of the *trans*-form of the azobenzene chromophore. The maximum absorption wavelength (λ_{max}) shifted to a shorter wavelength (hypsochromic shift) with an increase in the electron-donating ability of the substituent. The broad absorption bands due to the $n - \pi^*$ transitions of the *cis*-isomer of the azobenzene chromophore are located at ~ 500 nm at room temperature, irrespective of the substituent, except for the amino substituent. The *cis*-form of **AmCzE** clearly appears at 443 nm, which is a specific characteristic of aminoazobenzene-type molecules in which the $\pi - \pi^*$ and $n - \pi^*$ transitions nearly overlap.[35] The spectral features of the *trans*- and *cis*-forms were assigned by a spectral simulation of a first-principle molecular dynamics method (B3LYP/6-31G(d)). For the **ACzE**/PMMA films, the position of the isosbestic point, in which the spectra of the *trans*-to-*cis* isomerization overlap, was also estimated by the spectral simulation. Azobenzenes can be classified into three spectroscopic classes: azobenzene-type molecules, aminoazobenzene-type molecules and pseudo-stilbenes.[36] The features of pseudo-stilbene absorption spectra are significantly bathochromic-shifted, and the *cis*-isomer has an extremely short half-life. Accordingly, **ACzEs** should be classified as pseudo-stilbenes if they exhibit a bathochromic shift, their *cis*-form has a short half-life, and the changes in their spectra representing the *trans*–*cis* photoisomerization are not clearly probed.

The 3D-optimized electronic structure of the *trans*-isomer of each of the **ACzEs** in the ground state computed with the AM1 semi-empirical method are also shown in Figure 1. The negative phase of the wave function is illustrated in blue, and the positive phase is in red. All calculations referred to isolated molecules (gas phase). The geometry optimization was performed by minimizing the binding energy of the molecule. The HOMO (frontier molecular orbitals) as an electron donor reflects the ability of the molecule to donate an
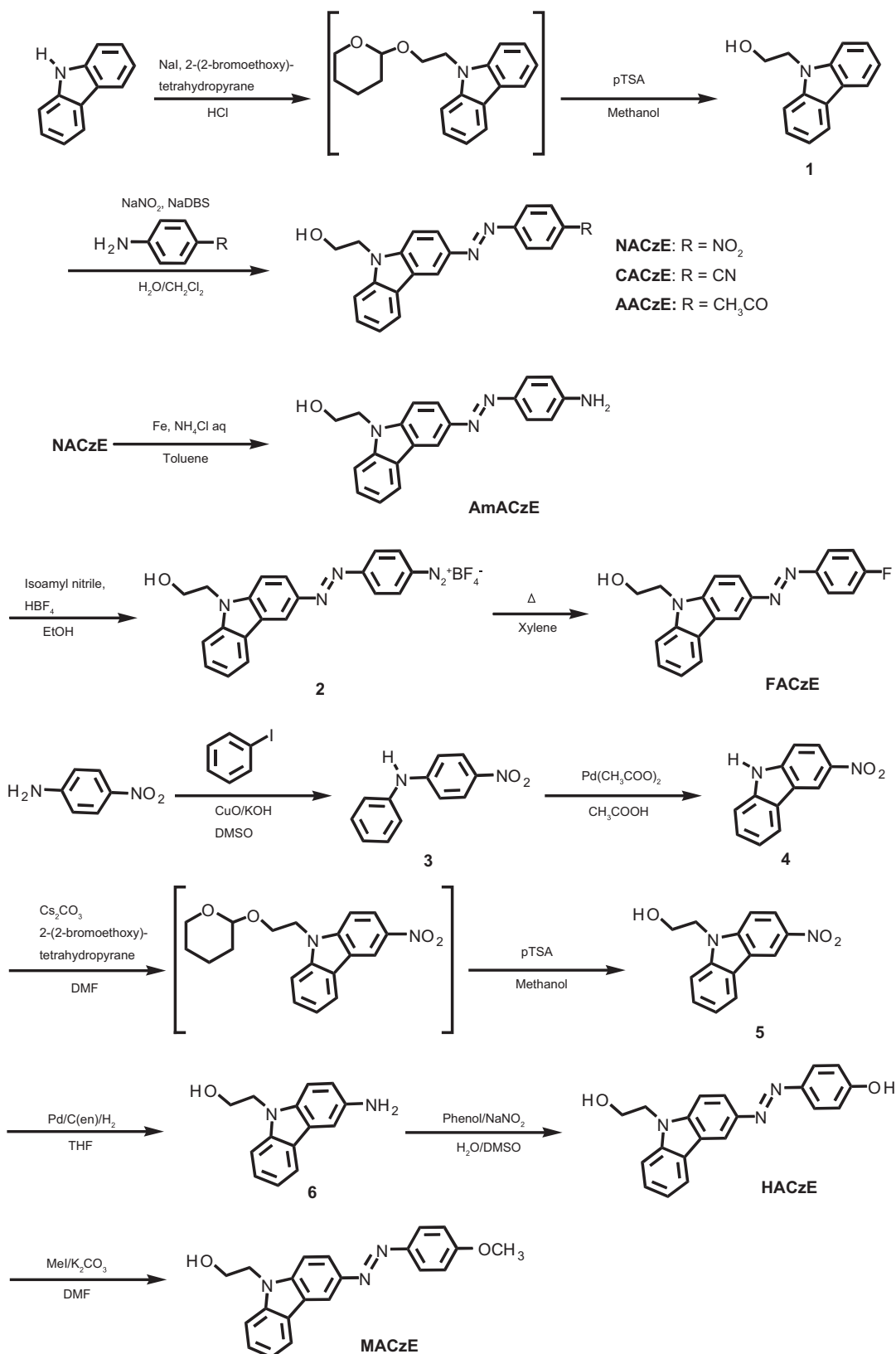
Scheme 1 Synthetic procedure for ACzEs.

electron. The π-electron cloud of the HOMO is primarily spread over the carbazole ring and azobenzene chromophore. Similar distributions of HOMOs were obtained for all of the **ACzEs**. The frontier molecular orbitals are shown on the 3D-optimized structures of the *trans*-isomers to provide a better understanding of the effect of the substituent on the energy levels and absorption spectra of the **ACzEs**.
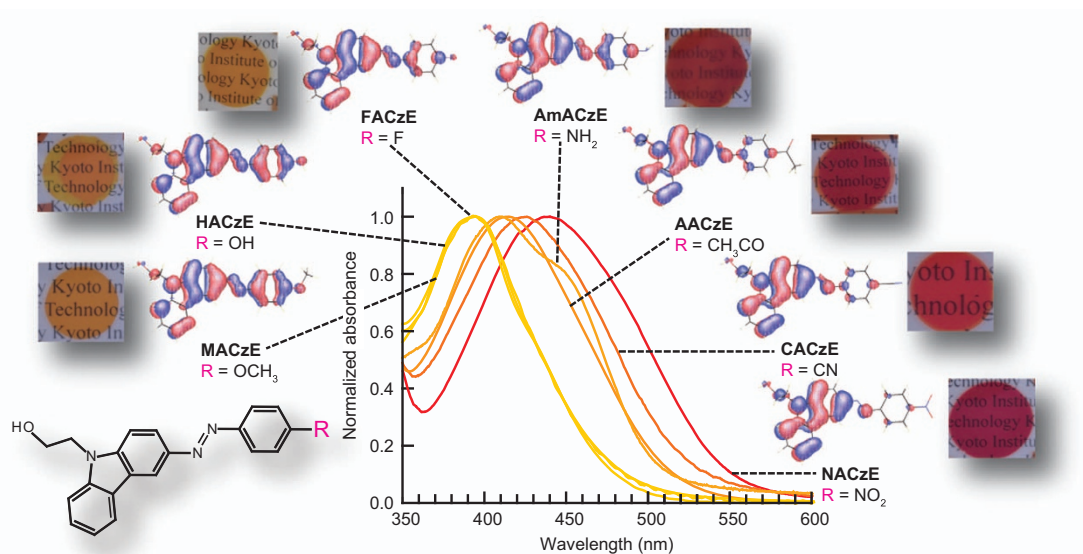
Figure 1 Absorption spectra, photograph of film and frontier molecular orbitals for ACzE/PMMA films. Absorption spectra of the **ACzE**/PMMA films (center). 3D-optimized structures and representations of the frontier molecular orbitals (HOMO) of the *trans*-isomers of the **ACzE**s computed by the AM1 method (around the absorption spectra). Photographs of a test piece of each **ACzE**/PMMA film (outer ring). Structure of the azobenzene-carbazole monolithic chromophores, 3-(phenylazo)-9*H*-carbazole-9-ethanols (**ACzEs**) (bottom left).
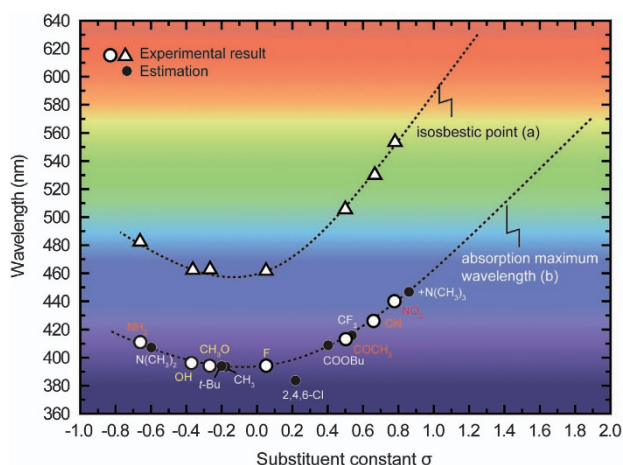

Figure 2 Plots of the absorption maximum wavelength and isosbestic point. Experimentally measured isosbestic point (a) and absorption maximum wavelength (b) are plotted as a function of the Hammett constant σ of each substituent in **ACzE**. Both the isosbestic point and absorption maximum wavelength have minimum values at a Hammett constant of $\sigma = 0$ for hydrogen substituents (unsubstituted **ACzE**). The dashed curve is a guide for the eye.

The HOMOs are delocalized over the carbazole and N=N chromogen, whereas the LUMOs (lowest unoccupied orbitals) are predominantly localized over the substituent phenyl ring. The addition of electron-withdrawing substituents, such as NO_2, CN, $COCH_3$ and F, lowers the energies of the unoccupied levels, which leads to the bathochromic shift. Conversely, the addition of electron-donating groups, such as OCH_3, OH and NH_2, decreases the ground-state dipole moment, which lowers the energies of the HOMOs. Therefore, the addition of stronger electron-donating substituents generally leads to a larger HOMO–LUMO gap (hypsochromic shift in the absorption spectra). Photographs of the **ACzE**/PMMA films are also shown in Figure 1.

The effect of substituents on the physicochemical properties of a series of related compounds with different substituents is quantitatively related to Hammett constants σ.[37] The absorption maximum (λ_{max}) depends on the nature of the substituent. The isosbestic point (λ_{iso}) and λ_{max} of the series of **ACzE** compounds with different substituents are plotted as a function of the σ of the substituents in Figure 2. Due to electron-accepting groups, a positive relation between σ and λ_{max} can be observed in the region of positive σ.

The bathochromic shift was measured with increasing σ values at $\sigma > 0$: $\lambda_{max} = 394$ nm at $\sigma = 0.006$ for the F substituent and $\lambda_{max} = 440$ nm at $\sigma = 0.778$ for the NO_2 substituent. A negative relation between λ_{max} and σ can be observed in the negative σ region due to electron-donating groups. A V-shaped Hammett relation was then obtained, which has also been experimentally reported for substituted azobenzene.[38,39] Substituents with positive σ accelerate the chemical reaction, whereas substituents with negative σ decelerate the reaction.

When the electron donating ability of the substituent is stronger in the region of negative Hammett constants, a bathochromic shift of λ_{max} is also observed: $\lambda_{max} = 388$ nm at $\sigma = -0.170$ for the CH_3 substituent and $\lambda_{max} = 410$ nm at $\sigma = -0.660$ for the NH_2 substituent. The positive and negative relations between λ_{max} and σ indicate that the charge transfer between the two rings of the carbazole and benzene moieties occurs in both the positive direction and inverse direction, depending on the substituent. Namely, with electron-accepting substituents, electrons are intensely withdrawn from the carbazole to benzene moieties. With electron-donating substituents, weak withdrawal occurs from the benzene to carbazole moieties. Accordingly, the **ACzE**s on the same slopes have the same electronic transition mechanism.

Similar relations between the λ_{iso} and Hammett constants σ are presented for the **ACzE**s in the PMMA films. The excitation at the λ_{iso} intensely promotes the Weigert effect[40] because the excitation at λ_{iso} can efficiently switch between the two isomer states, *trans* and *cis*. When **ACzE** is irradiated by a linearly or circularly polarized light, the

Table 1 Holographic and film properties of the ACzE/PMMA films relative to the writing beam wavelength

Dye	λ (nm)	n	α (cm⁻¹)	η (%)	τ (s)	S (cm² J⁻¹)	d (μm)	Δθ₀ (degree)	Q	R/B
NACzE	473	1.67	>8000	0.0	—	—	—	—	—	—
	491	1.63	>8000	0.0	—	—	—	—	—	—
	532	1.59	>8000	12.6	18.6	0.0290	8.2	14.1	4	R,B
	561	1.58	2476	82.7	17.9	0.1580	22.9	5.4	10	B
	594	1.57	320	68.6	60.7	0.0280	37.1	3.5	15	B
	633	1.57	84	16.1	156.0	0.0090	36.6	3.8	14	B
CACzE	473	1.72	>8000	0.0	—	—	—	—	—	—
	491	1.67	>8000	4.1	2.1	0.1910	7.1	15.2	4	R,B
	532	1.62	1729	68.3	5.4	0.2140	25.4	4.6	12	B
	561	1.60	322	88.0	10.2	0.2630	51.3	1.9	22	B
	594	1.59	85	28.3	59.2	0.0170	49.7	2.1	20	B
	633	1.59	73	0.0	—	—	—	—	—	—
AACzE	473	1.72	>8000	4.8	6.7	0.0600	4.0	25.8	2	R,B
	491	1.67	>8000	7.4	8.5	0.0740	8.0	13.5	4	R,B
	532	1.62	1402	76.4	20.4	0.0700	33.6	3.5	16	B
	561	1.60	286	69.4	26.3	0.1060	50.9	2.4	22	B
	594	1.59	69	90.2	156.3	0.0130	44.9	2.9	18	B
	633	1.59	34	0.0	—	—	—	—	—	—
MACzE	473	1.67	>8000	6.8	4.5	0.1170	9.5	11.2	5	R,B
	491	1.65	2375	23.6	13.9	0.0887	23.9	4.6	12	B
	532	1.61	201	43.6	18.1	0.0653	45.9	2.1	21	B
	561	1.59	86	13.8	309.0	0.0044	47.3	2.5	21	B
	594	1.59	68	0.0	—	—	—	—	—	—
	633	1.59	64	0.0	—	—	—	—	—	—
HACzE	473	1.72	>8000	7.2	7.8	0.0630	11.6	8.9	6	R,B
	491	1.67	2362	19.6	11.3	0.0900	18.6	5.8	10	B
	532	1.62	366	33.8	39.7	0.0240	60.8	2.0	28	B
	561	1.60	96	23.3	315.1	0.0050	60.1	2.0	26	B
	594	1.59	54	0.0	—	—	—	—	—	—
	633	1.59	37	0.0	—	—	—	—	—	—
AmACzE				No diffraction due to scattering						
triCl-ACzE[41]	532	—	<100	ca. 80	ca. 30	—	—	—	—	—
DR1[46])	532	—	>8000	ca. 0.1	ca. 10	—	—	—	—	—

Abbreviations: λ, wavelength of laser; n, refractive index; α, absorption coefficient; η, diffraction efficiency; τ, response time (grating formation time); S, sensitivity; d, grating thickness; Δθ, angular deviation from the Bragg angle; Q, Q-factor defined by equation (8); R/B, R = Intermingled Bragg and Raman–Nath (1 ⩽ Q ⩽ 10), B = Bragg (Q > 10).
The laser intensity at each wavelength is also listed.
Writing beam intensity: 473 nm (0.474 W cm⁻²); 491 nm (0.377 W cm⁻²); 532 nm (0.535 W cm⁻²); 561 nm (0.261 W cm⁻²); 594 nm (0.394 W cm⁻²); 633 nm (0.221 W cm⁻²).

transition moment parallel to the light polarization in **ACzE** is selectively excited. Combining the polarization-selective forward *trans*-to-*cis* photoisomerization and the unselective backward *cis*-to-*trans* photoisomerization, the number of **ACzE**s with their transition moments normal to the light polarization direction gradually increases, resulting in light-selective alignment, with the transition moments of the **ACzE**s almost perpendicular to the polarization direction of the actinic light. Through these processes, the photo-alignment and subsequent reorientation of **ACzE** occurs quickly, which changes the refractive index. Thus, the selective excitation at the λ_{iso} provides the specified holographic features that can be used to optimize the performance of updatable holograms.

Wavelength dependence of the writing beam
As discussed above, the λ_{iso} is an appropriate wavelength for hologram writing. To ensure the veracity of the above discussion, the dependence of the writing beam wavelength on the rewritable holographic properties was investigated. The time dependence of the diffraction efficiencies as a function of the writing beam wavelength for the

ACzE/PMMA films was investigated. The response time of the diffraction is commonly used to evaluate the time required for the grating formation. To estimate the response time (grating formation time) τ for the respective writing beam wavelengths, the diffraction efficiencies as a function of time were fitted by the Kohlrausch–Williams–Watts-stretched exponential function shown in equation (2).

$$\eta\% = \eta_0 \left\{ 1 - \exp\left[-\left(\frac{t}{\tau}\right)^{\beta} \right] \right\} \tag{2}$$

For the **ACzE**/PMMA films, the diffraction efficiencies and response times are shown in Table 1. Unfortunately, the holographic properties of **FACzE**/PMMA could not be evaluated because of a material shortage. For comparison, the holographic properties of the related materials are also listed at the bottom of Table 1. The rate of *trans*–*cis* photoisomerization depends on the free volume around the dyes as well as the interaction between the host matrix and the dye molecules, but it is also substantially affected by the writing beam wavelength. Thus, the writing beam wavelength is highly related to the rate-

determining process for the grating formation in **ACzE**/PMMA films. For pseudo-stilbenes, the rate of the grating formation should be controlled by the quantum efficiency of the *trans–cis* photoisomerization and the half-life of the *cis*-form. Therefore, for the **ACzEs**, excitation at an isosbestic point is in good agreement with the faster response time for the holographic diffraction. The maximum holographic response obviously occurs at a wavelength near the λ_{iso}.

Total holographic performance is commonly evaluated using sensitivity *S*, which is defined as follows:

$$S = \frac{\sqrt{\eta'}}{I \cdot \tau} \tag{3}$$

where η' is an effective diffraction efficiency ($\eta' = \exp(-\alpha_{632.8}L/\cos\theta)$ η, where $\alpha_{632.8}$ is the absorption coefficient at 632.8 nm, *L* is the sample thickness and θ is the internal angle (here $\theta = 0°$)) considering the optical losses due to the absorption at the wavelength of the reading beam, τ is the response time and *I* is the writing beam intensity.

The obtained sensitivities, *S*, gave the appropriate writing beam wavelengths for the respective **ACzE**/PMMA films as follows: 561 nm for **NACzE**, 532 nm or 561 nm for **CACzE** and **AACzE**, and 491 nm for **MACzE** and **HACzE**.

The reading beam wavelength is an important deciding factor of a hologram's color. Theoretically, use of the same wavelength for writing and reading is preferred. However, from the standpoint of the absorption spectra of the chromophores, the color of the hologram is restricted by longer wavelengths than the writing beam wavelength. An absorption coefficient of $<300\ \text{cm}^{-1}$ should be selected for the reading beam wavelength to avoid strong absorption of the reading beam. Thus, it is preferable to select a red reading beam for **NACzE**; red or yellow reading beams for **CACzE** and **AACzE**; and red, yellow, and green reading beams for **MACzE** and **HACzE**.

To reproduce high-quality holograms for holographic display devices independently of the magnification factor, high transparency and no scattering are required. Therefore, stability, fatigue resistance and durability of the sample films become important factors. For stability, we used all of the sample films without observing any deterioration because a wavelength in the region of visible light, primarily the isosbestic point wavelength, (not ultraviolet light) was adopted as the writing beam. For this reason, the present samples are not deteriorated by light, unlike a typical photochromic system, which degrades the holographic properties by light illumination. The fatigue resistance, which is related to the stability, of the samples was excellent. When the hologram was recorded and erased and recorded again, the diffraction efficiency was the same and the response time was not changed. We repeated these procedures several times and holographic performances did not deteriorate. We confirm that the **ACzEs**/PMMA exhibit excellent durability of 2–3 years or more. Haze value (%), defined by the ratio of diffuse transmittance (%)/total light transmittance (%) × 100, was measured for **ACzEs**/PMMA films. The obtained average haze value of the **ACzEs**/PMMA films was 4% except for the **AmACzE**/PMMA film (haze% = 67%), which can be maintained for 2–3 years. These results indicate that dye aggregation or phase separation did not occur. We propose here that the haze value of updatable full-color holographic displays is preferably 4% or below.

Angle dependence of the writing beam

Volume holograms are categorized as transmission and reflection holograms. In transmission holograms, the grating planes are normal to the surface of the holographic medium. For the writing of such

holograms, two writing beams (object and reference beams) enter from the same side of the sample surface. These holograms can be reproduced by transmitting a beam of light through the holographic medium. Transmission holograms have a high angular selectivity.[41,42] In reflection holograms, the grating planes are parallel to the surface of the hologram medium. For the recording of such holograms, the object and reference beams enter from opposite sides of the holographic recording medium. These holograms can be reproduced by reflecting a beam from the grating planes in the holographic recording medium. Such holograms are known to have a high spectral selectivity.[43] To optimize the performance of the writing beam wavelength for rewritable holograms, the angular selectivity of recorded holograms should be evaluated relative to the writing beam wavelength. A coupled-wave analysis proposed by Kogelnik[44] was introduced to predict the relationship between the incident angle and diffraction efficiency in thick gratings. The angular selectivities of recorded gratings for different writing beam wavelengths are shown in Figure 3. The diffraction efficiency η for the symmetric gratings and the lossless transmission gratings is defined[44] as

$$\eta = \frac{\sin^2\sqrt{v^2 + \xi^2}}{1 + \xi^2/v^2} = v^2 \sin c^2\sqrt{v^2 + \xi^2} \tag{4}$$

where $\text{sinc}(x) = \sin(x)/x$. The variables ν and ξ are as defined in Kogelnik *et al.*[44] where ν is the grating strength,

$$v = \frac{\pi n d}{\lambda \cos\theta_0} \tag{5}$$

and

$$\xi = \Delta\theta \frac{\pi d}{\Lambda} \tag{6}$$

is related to the angular deviation from the Bragg angle $\Delta\theta$. For weakly modulated gratings ν ($\ll\ll\xi$),

$$\eta = v^2 \sin c^2(\xi) \tag{7}$$

The grating thicknesses *d* in the **ACzE**/PMMA films were obtained from curve fitting the angular selectivity measurements of the recorded gratings shown in Figure 3. The obtained angular dependences for the **ACzE**/PMMA films are also summarized in Table 1. A shorter writing beam wavelength, an absorption coefficient α much $>8000\ \text{cm}^{-1}$ or a grating thickness $<10\ \mu\text{m}$ is better for each sample film, considering a wide viewing angle. However, from the point of view of higher sensitivity *S* and a diffraction efficiency of $>20\%$, the appropriate grating thickness is ca. $20\ \mu\text{m}$. Furthermore, when the writing beam wavelength is near the isosbestic point, the absorption coefficients α of the **ACzE**/PMMA films at the writing beam wavelength are in the range of 286–$2476\ \text{cm}^{-1}$, which is more appropriate for holographic recordings.

A grating can be classified as a volume (or thick) and planar (or thin) hologram. A hologram is considered thick if the thickness of the recording medium is greater than the spacing between the interference fringes. Otherwise, the hologram is considered to be thin. A dimensionless analytic factor, the *Q*-factor, helps to distinguish between the two types of holograms.[45] The *Q*-factor is defined as

$$Q = \frac{2\pi\lambda d}{n\Lambda^2} \tag{8}$$

where *d* is the thickness of the recording grating, *n* is the refractive index of the recording grating, λ is the writing beam wavelength and Λ is the spacing between the grating period. The obtained *Q*-factors are also shown in Table 1. If $Q > 10$, only one strong diffraction order is
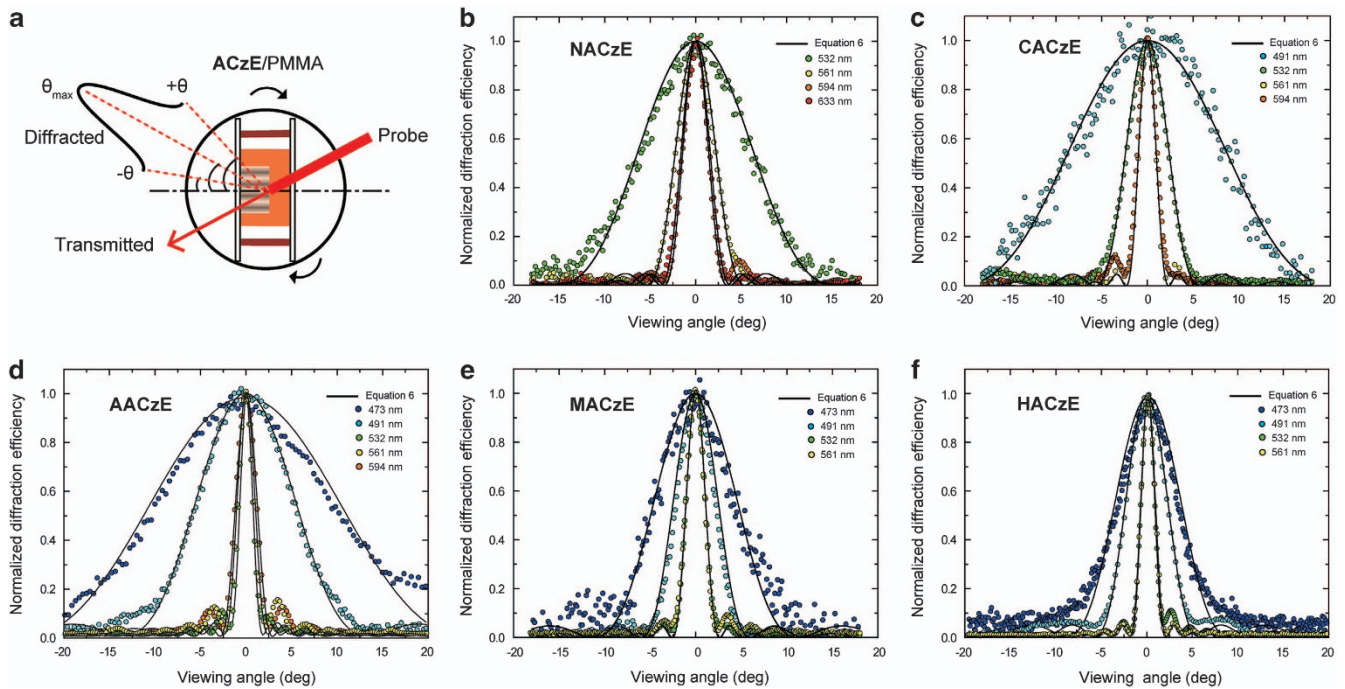
Figure 3 Normalized diffraction efficiencies as a function of the viewing angle in air. (**a**) Schematic illustration for viewing angle dependence of diffracted beam in **ACzE**/PMMA. (**b**) **NACzE**, (**c**) **CACzE**, (**d**) **AACzE**, (**e**) **MACzE** and (**f**) **HACzE**. The wavelength shown in each figure is the recording wavelength. The reading wavelength for all the **ACzE**/PMMA samples is 632.8 nm. The experimental data are fitted by the theoretical plots (solid curve) using equation (7). For all samples, the viewing angle becomes wider when the recording wavelength becomes shorter because of shallower grating depth due to the large absorption coefficient.
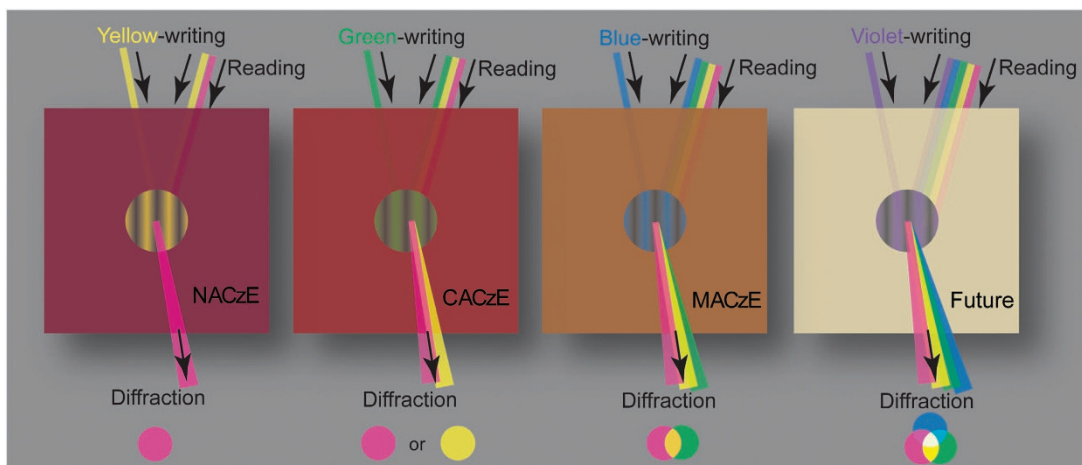
Figure 4 Schematic representations of beam colors for recording and reading each of the **ACzE**/PMMA films. **NACzE**/PMMA: yellow color recording and red color reading. **CACzE**/PMMA: green color recording and red or yellow color reading. **MACzE**/PMMA: blue color recording and red, yellow and green color reading. Future sample: violet color recording and red, yellow, green and blue color reading. The **NACzE**/PMMA and **CACzE**/PMMA films are designed for an updatable mono-color hologram. The **MACzE**/PMMA film is designed for an updatable multi-color hologram using red and green laser beams. The future sample may be effective for an updatable full-color hologram using red, green and blue laser beams. A practical updatable multi-color hologram in **MACzE**/PMMA film is shown in Figure 5.

observed, and the Bragg condition is satisfied. If $Q < 1$, multiple diffraction orders are observed, and this type of diffraction is called the Raman–Nath condition. In addition to the above two critical conditions, an intermediate Q-factor region, $1 \leqslant Q \leqslant 10$, is assumed to be an intermingled regime of the Bragg condition and the Raman–Nath condition. Consequently, the appropriate holographic properties appear in an intermingled Bragg and Raman–Nath regime with a Q-factor of $1 \leqslant Q \leqslant 10$ and a Bragg condition of $Q > 10$.

On the basis of a comprehensive assessment of these spectroscopic and holographic optical results, a schematic representation of the appropriate writing and reading beams is shown in Figure 4 for **NACzE**, **CACzE** and **MACzE**: the appropriate writing beam wavelengths are 561 nm for **NACzE**, 532 nm for **CACzE** and 491 nm for **MACzE**; the appropriate reading beams are a red reading beam with a wavelength longer than 600 nm for **NACzE**; red or yellow reading beams with wavelengths longer than 560 nm for **CACzE**; and
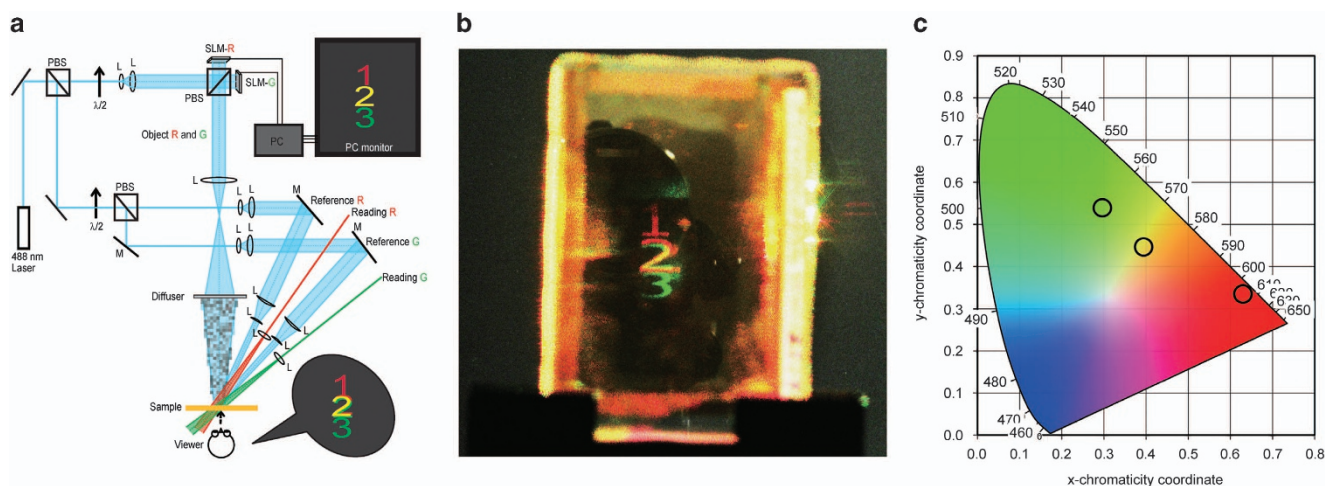
8

Figure 5 Multi-color holographic recording and reading system, reproduced multi-color hologram and chromaticity diagram. (**a**) Setup for multi-color hologram recording and reading system. λ/2, half wave plate; L, lens; M, mirror; PBS, polarizing beam splitter; PC, computer; SLM, spatial light modulator. (**b**) Photograph of reproduced multi-color hologram. Red ('1'), yellow ('2') and green ('3') numerals are clearly reproduced in the updatable hologram with each color. (**c**) CIE1931 chromaticity diagram at the maximum brightness. Color coordinates of the reconstructed holograms '1', '2' and '3' are shown as open circles.

red, yellow, and green reading beams with wavelengths longer than 530 nm for **MACzE**. The simultaneous illumination of red and green reading beams displays the multi-color hologram corresponding to the respective reading beam. Multi-color hologram reproduction using a **MACzE**/PMMA is shown in Figure 5. The updatable holographic display system for a multi-color hologram is shown in Figure 5a: the original image is divided into red and green color images through a video signal splitter. Each image on a spatial light modulator is individually recorded in the **MACzE**/PMMA film device using a single longitudinal mode blue laser. Each hologram is reproduced using a green laser and a red laser to synthesize the color hologram. A clear multi-color hologram of red ('1') yellow ('2') and green ('3') numerals can be reproduced with red and green reading laser beams as shown in Figure 5b. The CIE1931 chromaticity diagram at the maximum brightness is also shown in Figure 5c. Circles in the figure correspond to colors in the hologram. A recent study determined that 2,4,6-trichloro (Cl)-substituted **ACzE** presents an absorption peak at 384 nm.[46] A green-colored hologram was produced using a PMMA film containing the trichloro-substituted **ACzE**. Using the present approach, we can predict that holograms using unsubstituted **ACzE** can be written by a violet light and read by a blue light (future in Figure 4). The synthesis of unsubstituted **ACzE** is challenging and a target of future research.

CONCLUSIONS
Seven types of azo-carbazole (**ACzE**) monolithic dyes were synthesized. The influence of substituents introduced in the *para* position of the phenyl ring and the distinct strength of the substituents (NO$_2$, CN, CH$_3$CO, F, CH$_3$O, OH and NH$_2$) on the phenyl ring of the **ACzEs** were investigated on the basis of spectroscopic and holographic optical aspects. The experimental evidence strongly suggests that the appropriate writing beam wavelengths are 561 nm for **NACzE**, 532 nm for **CACzE** (and **AACzE**) and 491 nm for **MACzE** (and **HACzE**). The appropriate wavelengths for the reading beams are longer than 600 nm for **NACzE,** longer than 560 nm for **CACzE** (and **AACzE**) and longer than 530 nm for **MACzE** (and **HACzE**).

Material design that is suitable for updatable full-color holography is highly challenging, but very attractive and advantageous for many practical applications such as digital signage.

1 Ikeda, T. Photomodulation of liquid crystal orientations for photonic applications. *J. Mater. Chem.* **13**, 2037–2057 (2003).
2 Nathanson, A. & Rochon, P. Photoinduced motions in azo-containing polymers. *Chem. Rev.* **102**, 4139–4176 (2002).
3 Hagen, R. & Bieringer, T. Photoaddressable polymers for optical data storage. *Adv. Mater.* **13**, 1805–1810 (2001).
4 Matharu, A. S., Jeeva, S. & Ramanujam, P. S. Liquid crystals for holographic optical data storage. *Chem. Soc. Rev.* **36**, 1868–1880 (2007).
5 Rad, J. K., Mahdavian, A. R., Salehi-Mobarakeh, H. & Abdollahi, A. FRET phenomenon in photoreversible dual-color fluorescent polymeric nanoparticles based on azocarbazole/spiropyran derivatives. *Macromolecules* **49**, 141–152 (2016).
6 Todorov, T., Nikolova, L. & Tomova, N. Polarization holography. 1: A new high-efficiency organic material with reversible photoinduced birefringence. *Appl. Opt.* **23**, 4309–4312 (1984).
7 Sasaki, T., Ono, H. & Kawasaki, N. Functionalized polarization gratings in azo-dye-doped polymer films. *Mol. Crsyt. Liq. Cryst.* **472**, 131–136 (2007).
8 Harada, K., Itoh, M., Yatagai, T. & Kamemaru, S. Application of surface relief hologram using azobenzene containing polymer film. *Opt. Rev.* **12**, 130–134 (2005).
9 Sasaki, T., Ikegami, M., Abe, T., Miyazaki, D., Kajikawa, S. & Naka, Y. Real-time dynamic hologram in photorefractive ferroelectric liquid crystal with two-beam coupling gain coefficient of over 800 cm^{-1} and response time of 8 ms. *Appl. Phys. Lett.* **102**, 063306–063309 (2013).
10 Williams, C., Montelongo, Y., Tenorio-Pearl, J. O., Cabrero-Vilatela, A., Hofmann, S., Milne, W. I. & Wilkinson, T. D. Engineered pixels using active plasmonic holograms with liquid crystals. Physica status Solidi (RRL). *Rapid Res. Lett.* **9**, 125–129 (2015).
11 Mao, W., Sun, Q., Baig, S., Lu, H. & Wang, M. R. Red light holographic recording and readout on an azobenzene–LC polymer hybrid composite system. *Opt. Commun.* **355**, 256–260 (2015).

12 Zeng, P., Wang, C., Zhao, F., Cai, P. & Qin, M. Polarization-controlled images based on double-exposure polarization holography in an azobenzene liquid-crystalline polymer. *Appl. Opt.* **54**, 54–59 (2015).

13 Shishido, A. Rewritable holograms based on azobenzene-containing liquid-crystalline polymers. *Polym. J.* **42**, 525–533 (2010).

14 Su, Y.-C., Chu, C.-C., Chang, W.-T. & Hsiao, V. K. S. Characterization of optically switchable holographic polymer-dispersed liquid crystal transmission gratings. *Opt. Mater.* **34**, 251–255 (2011).

15 Eich, M. & Wendorff, J. H. Erasable holograms in polymeric liquid crystals. *Makromol. Chem. Rapid Commun.* **8**, 467–471 (1987).

16 Tsujimura, S., Kinashi, K., Sakai, W. & Tsutsumi, N. High-speed photorefractive response capability in triphenylamine polymer-based composites. *Appl. Phys. Express* **5**, 064101 (2012).

17 Tsujimura, S., Kinashi, K., Sakai, W. & Tsutsumi, N. Recent advances in photorefractivity of poly(4-diphenylamino)styrene composites: wavelength dependence and dynamic holographic images. *Jpn J. Apply. Phys.* **53**, 082601 (2014).

18 Giang, H. N., Kinashi, K., Sakai, W. & Tsutsumi, N. Photorefractive response and real-time holographic application of a poly(4-(diphenylamino)benzyl acrylate)-based composite. *Polym. J.* **46**, 59–66 (2014).

19 Blanche, P.-A., Bablumian, A., Voorakaranam, R., Christenson, C., Lin, W., Gu, T., Flores, D., Wang, P., Hsieh, W.-Y., Kathaperumal, M., Rachwal, B., Siddiqui, O., Thomas, J., Norwood, R. A., Yamamoto, M. & Peyghambarian, N. Holographic three-dimensional telepresence using large-area photorefractive polymer. *Nature* **468**, 80–83 (2010).

20 Schab-Balcerzak, E., Grabiec, E., Sek, D. & Miniewicz, A. New azobenzene chromophores as monomers for synthesis of polyesters. *Polym. J.* **35**, 851–858 (2003).

21 Wang, C., Fai, H., Yang, Y., Wei, Z., Qiu, Y. & Chen, Y. Photoinduced anisotropy and polarization holography in azobenzene side-chain polymer. *Opt. Commun.* **159**, 58–62 (1999).

22 Natansohn, A. & Rochon, P. Photoinduced motions in azobenzene-based amorphous polymers: possible photonic devices. *Adv. Mater.* **11**, 1387–1391 (1999).

23 Ramanujam, P. S., Pedersen, M. & Hvilsted, S. Instant holography. *Appl. Phys. Lett.* **74**, 3227–3229 (1999).

24 Wu, Y., Natansohn, A. & Rochon, P. Photoinduced birefringence and surface relief gratings in polyurethane elastomers with azobenzene chromophore in the hard segment. *Macromolecules* **37**, 6090–6095 (2004).

25 Kinashi, K., Kambe, Y., Misaki, M., Koshiba, Y., Ishida, K. & Ueda, Y. Synthesis, characterization, photo-induced alignment, and surface orientation of poly(9,9-dioctyl-fluorene-alt-azobenzene)s. *J. Polym. Sci. A Polym. Chem.* **50**, 5107–5114 (2012).

26 Pietsch, U., Rochon, P. & Natansohn, A. Formation of a buried lateral density grating in azobenzene polymer films. *Adv. Mater.* **12**, 1129–1132 (2000).

27 Tsutsumi, N., Kinashi, K., Sakai, W., Nishide, J., Yutaka Kawabe, Y. & Sasabe, H. Real-time three-dimensional holographic display using a monolithic organic compound dispersed film. *Opt. Mater. Express* **2**, 1003–1010 (2012).

28 Tsutsumi, N., Kinashi, K., Tada, K., Fukuzawa, K. & Kawabe, Y. Fully updatable three-dimensional holographic stereogram display device based on organic monolithic compound. *Opt. Express* **21**, 19880–19884 (2013).

29 Tsutsumi, N., Kinashi, K., Ogo, K., Fukami, T., Yabuhara, Y., Kawabe, Y., Tada, K., Fukuzawa, K., Kawamoto, M., Sassa, T., Fujihara, T., Sasaki, T. & Naka, Y. Updatable holographic diffraction of monolithic carbazole-azobenzene compound in poly(methyl methacrylate) matrix. *J. Phys. Chem. C* **119**, 18567–18572 (2015).

30 Prime, M. E., Andersen, O. A., Barker, J. J., Brooks, M. A., Cheng, R. K. Y., Toogood-Johnson, I., Courtney, S. M., Brookfield, F. A., Yarnold, C. J., Marston, R. W., Johnson, P. D., Johnsen, S. F., Palfrey, J. J., Vaidya, D., Erfan, S., Ichihara, O., Felicetti, B., Palan, S., Pedret-Dunn, A., Schaertl, S., Sternberger, I., Ebneth, A., Scheel, A., Winkler, D., Toledo-Sherman, L., Beconi, M., Macdonald, D., Muñoz-Sanjuan, I., Dominguez, C. & Wityak, J. Discovery and structure-activity relationship of potent and selective covalent inhibitors of transglutaminase 2 for Huntington's disease. *J. Med. Chem.* **55**, 1021–1046 (2012).

31 Laali, K. K. & Gettwert, V. J. Fluorodediazoniation in ionic liquid solvents: new life for the Balz–Schiemann reaction. *J. Fluorine Chem.* **107**, 31–34 (2001).

32 Ullmann, F. & Bielecki, J. Ueber Synthesen in der Biphenylreihe. *Ber. Dtsch. Chem. Ges.* **34**, 2174–2185 (1901).

33 Tanaka, A., Nishide, J. & Sasabe, H. Asymmetric energy transfer in photorefractive polymer Composites. *Mol. Cryst. Liq. Cryst.* **504**, 44–51 (2009).

34 Matsuoka, T., Tada, K., Yoshikawa, T. & Kawabe, Y. Optically inscribed grating in azo-carbazole dye: concentration dependence. *Surf. Sci. Nanotechnol.* **13**, 69–74 (2015).

35 Rau, H. in *Photochemistry and Photophysics* Vol. 2 (ed. Rebek, J.) 119–141 (CRC Press, Boca Raton, FL, USA, 1990).

36 Rau, H. in *Photoreactive Organic Thin Films* (eds Sekkat, Z. & Knoll, W.) 3–47 (Academic Press, Amsterdam, Netherlands, 2002).

37 Hansch, C., Leo, A. & Taft, R. W. A survey of Hammett substituent constants and resonance and field parameters. *Chem. Rev.* **91**, 165–195 (1991).

38 Dokić, J., Gothe, M., Wirth, J., Peters, M.V., Schwarz, J., Hecht, S. & Saalfrank, P. Quantum chemical investigation of thermal cis-to-trans isomerization of azobenzene derivatives: substituent effects, solvent effects, and comparison to experimental data. *J. Phys. Chem. A* **113**, 6763–6773 (2009).

39 Nishimura, N., Sueyoshi, T., Yamanaka, H., Imai, E., Yamamoto, S. & Hasegawa, S. Thermal cis-to-trans isomerization of substituted azobenzenes II. Substituent and solvent effects. *Bull. Chem. Soc. Jpn* **49**, 1381–1387 (1976).

40 Weigert, F. Dichroism induced in a fine–grain silverchloride emulsion by a beam of linearly polarized light. *Verh. Dtsch. Phys. Ges.* **21**, 479–483 (1919).

41 Ciapurin, I. V., Drachenberg, D. R., Smirnov, V. I., Venus, G. B. & Glebov, L. B. Modeling of phase volume diffractive gratings, part 2: Reflecting sinusoidal uniform gratings, Bragg mirrors. *Opt. Eng.* **51**, 058001 (2012).

42 Curtis, K. & Psaltis, D. Recording of multiple holograms in photopolymer films. *Appl. Opt.* **31**, 7425–7428 (1992).

43 Gallego, S., Neipp, C., Estepa, L. A., Ortuño, M., Márquez, A., Francés, J., Pascual, I. & Beléndez, A. Volume holograms in photopolymers: comparison between analytical and rigorous theories. *Materials* **5**, 1373–1388 (2012).

44 Kogelnik, H. Coupled wave theory for thick hologram gratings. *Bell Syst. Tech. J.* **48**, 2909–2947 (1969).

45 Akbari, H., Naydenova, I., Persechini, L., Garner, S. M., Cimo, P. & Martin, S. Diffractive optical elements with a large angle of operation recorded in acrylamide based photopolymer on flexible substrates. *Int. J. Polym. Sci.* **2014**, 918285 (2014).

46 Miura, S. & Kobayashi, S. New multicolor and rewritable holographic polymer film for three-dimensional holographic display. *J. Soc. Info. Display* **22**, 597–602 (2014).

Supplementary Information accompanies the paper on the NPG Asia Materials website (http://www.nature.com/am)